

Global Tests for Smoothed Functions in Mean Field Variational Additive Models

Mark J. Meyer and Junyi Wei

Department of Mathematics and Statistics, Georgetown University
Washington, DC USA

Abstract

Variational regression methods are an increasingly popular tool for their efficient estimation of complex. Given the mixed model representation of penalized effects, additive regression models with smoothed effects and scalar-on-function regression models can be fit relatively efficiently in a variational framework. However, inferential procedures for smoothed and functional effects in such a context is limited. We demonstrate that by using the Mean Field Variational Bayesian (MFVB) approximation to the additive model and the subsequent Coordinate Ascent Variational Inference (CAVI) algorithm, we can obtain a form of the estimated effects required of a Frequentist test for semiparametric curves. We establish MFVB approximations and CAVI algorithms for both Gaussian and binary additive models with an arbitrary number of smoothed and functional effects. We then derive a global testing framework for smoothed and functional effects. Our empirical study demonstrates that the test maintains good Frequentist properties in the variational framework and can be used to directly test results from a converged, MFVB approximation and CAVI algorithm. We illustrate the applicability of this approach in a wide range of data illustrations.

1 Introduction

Variational approximations cover a useful class of algorithms for calculating, in a deterministic fashion, estimates from Bayesian posterior distributions. One such class, the Mean Field Variational Bayesian (MFVB) approximation, has been well studied with many standard statistical models derived for use in the class, see for example Ormerod and Wand [2010] or Blei et al.

[2017]. Recent research suggests that estimates arising from MFVB share similar properties with their Frequentist counter-parts including the consistency and the asymptotic normality of variational estimators [Bickel et al., 2013, You et al., 2014, Wang and Blei, 2019, Westling and McCormick, 2019, Yang et al., 2020, Zhang and Zhou, 2020]. Such evaluations demonstrate that variational models have good Frequentist properties despite originating from a Bayesian estimation paradigm.

One understudied area, however, is in hypothesis testing. While percentile-based intervals can be constructed for parameters based on the conditional posterior, underestimation of the variance can result in misleading inference—particularly for non-normally distributed posteriors [Gelman et al., 2013, Giordano et al., 2018]. Some authors have proposed a bootstrap-based approach, see Chen et al. [2018], while others convert back to a fully Bayesian model when inference is of interest, for example Goldsmith and Kitago [2016]. For complicated variational regression models like additive models, performing both the modeling and inference in the same framework would be preferable to a more computationally burdensome approach of bootstrapping or running a separate, fully Bayesian estimation procedure. One such model is the additive model which typically implies a regression model with a scalar outcome and an additive smoothed or semiparametric effect or potentially a set of such effects in addition to scalar covariates

Additive models with smoothed effects have been broadly studied, see texts by Ruppert et al. [2003] or Wood [2017], for example. Variational Bayesian approaches that incorporate smoothing include work by Luts and Wand [2015], Lee and Wand [2016], Wand [2017], Hui et al. [2019], Yang and Yang [2024] and references therein. Methods that incorporate both smoothed and functional effects into non-variational additive models include the work of McLean et al. [2014], Scheipl et al. [2015, 2016], Li et al. [2016], Ma et al. [2021], among others. However, to our knowledge, there is no work examining variational additive models that accommodate an arbitrary number of both smoothed and functional effects. And while there is work on global testing for smoothed effects, see for example Zhang et al. [2000], Zhang and Lin [2003], Crainiceanu et al. [2005], Greven et al. [2008], Wood [2017], such tests have not been considered in the variational setting.

Global tests of the functional components in regression models are also limited. Much of the work has emphasized point-wise testing, see for example Malloy et al. [2010], Goldsmith et al. [2013] and Meyer et al. [2015]. Some authors have proposed global tests including Meyer et al. [2015] who exam-

ine an approach in a fully Bayesian function-on-function setting based on what the authors refer to as simultaneous band scores. Another example is Ivanescu et al. [2015] who note the connection between penalized functional effects and smoothed effects and suggest performing inference using an approach similar to Crainiceanu and Ruppert [2004] or Greven et al. [2008]. Neither authors explore the operating characteristics of their global tests for functional effects and such testing in the variational context has not been extensively studied.

In this manuscript, we explore MFVB approximations to variational additive models for both Gaussian and binary outcomes, developing Coordinate Ascent Variational Inference (CAVI) algorithms to perform estimation (Section 2). These models can incorporate an arbitrary number of both smoothed and functional effects and thus include semiparametric regression models (in the Ruppert et al. [2003] sense), scalar-on-function regression models (of the form described by Ramsay and Dalzell [1991] and Ramsay and Silverman [2005]), and the combination of the two. The target of inference we consider is either a smoothed effect or a functional effect, both of which can be represented as smoothed effects. Zhang et al. [2000] and Zhang and Lin [2003] propose a Frequentist-based test for semiparametric curves which we refer to as the ZLS test. We demonstrate that the CAVI algorithms for fitting MFVB approximations to both Gaussian and binary variational additive models admit forms required for the ZLS test which, we argue, can be used for a global test (Section 3). We explore the properties of the ZLS test, including the type I error rate and power, for global inference on both smoothed and functional effects arising from converged CAVI algorithms (Section 4). In Section 5, we demonstrate the use of the ZLS test in several data examples. Finally, we provide a discussion of the method in Section 6.

2 Statistical Framework

2.1 Mean Field Variational Bayesian Approximations

We begin with a brief overview of the MFVB approximation. Let $\boldsymbol{\theta}$ represent a vector of parameters and \mathbf{Y} represent a vector of observed data. The posterior distribution of $\boldsymbol{\theta}$ given the data, \mathbf{Y} , is then $p(\boldsymbol{\theta}|\mathbf{Y}) = p(\mathbf{Y}, \boldsymbol{\theta})/p(\mathbf{Y})$. The marginal distribution in the denominator, $p(\mathbf{Y})$, is typically intractable. Consequently, the posterior estimates must be obtained algorithmically. In

a fully Bayesian approach, this would involve a Markov Chain Monte Carlo simulation or some other iterative random sampling technique like Hamiltonian Monte Carlo, for example. The MFVB approach utilizes a density transformation approach that relies on the observation that, for an arbitrary density q , $p(\mathbf{Y})$ is bounded below by $\underline{p}(\mathbf{Y}; q)$ where $\underline{p}(\mathbf{Y}; q) = \exp \left[\int q(\boldsymbol{\theta}) \log \left\{ \frac{p(\mathbf{Y}, \boldsymbol{\theta})}{q(\boldsymbol{\theta})} \right\} d\boldsymbol{\theta} \right]$. The algorithms used to determine the approximations work by maximizing $\underline{p}(\mathbf{Y}; q)$ over a class of tractable densities, q . As $\underline{p}(\mathbf{Y}; q)$ is maximized, the Evidence Lower Bound (ELBO) will be minimized. The ELBO is a metric measuring the distance between the approximation, $q(\boldsymbol{\theta})$, and the posterior, $p(\boldsymbol{\theta}|\mathbf{Y})$, and is an equivalent, up to an additive constant, to the Kullback-Leibler or K-L Divergence.

For a partition of the parameter space $\boldsymbol{\theta}$ of size M , $\{\boldsymbol{\theta}_1, \dots, \boldsymbol{\theta}_M\}$, the MFVB approximation constructs $q(\boldsymbol{\theta})$ using a product density transformation of the form $q(\boldsymbol{\theta}) = \prod_{m=1}^M q_m(\boldsymbol{\theta}_m)$. Thus the resulting approximation is the product of the q -densities which are similar to the conditional posterior densities in a Gibbs sampling framework [Gelman et al., 2013]. Optimization occurs via an iterative process with convergence defined to occur when changes in the variational lower bound, $\underline{p}(\mathbf{Y}; q)$, become minimal. Minimizing the changes in $\underline{p}(\mathbf{Y}; q)$ in turn minimizes the ELBO, and therefore the KL divergence, between $q(\boldsymbol{\theta})$ and $p(\boldsymbol{\theta}|\mathbf{Y})$. To perform this optimization, the coordinate ascent variational inference (CAVI) algorithm is commonly used. Ormerod and Wand [2010] and Blei et al. [2017] provide detailed reviews and introductions to variational Bayesian techniques. Chapter 13 of Gelman et al. [2013] also gives a good introduction to the topic. While there are other variational approaches to approximating the posterior, our focus is on MFVB approximations obtained via CAVI. The relationship to the Gibbs sampling framework, where one component of $\boldsymbol{\theta}$ is updated at a time, means the algorithm will ultimately admit a useful form for the global test.

2.2 Variational Additive Models

2.2.1 Gaussian Outcome

Let y_i be the continuous outcome of interest for subjects $i = 1, \dots, n$. Each subject i has a scalar covariate response vector, \mathbf{x}_i , that is $p \times 1$. The intercept, α , and vector of non-smoothed, non-functional coefficients is $\boldsymbol{\beta}$ which is also $p \times 1$. Finally, we denote the model errors with ϵ_i and as-

sume $\epsilon_i \stackrel{iid}{\sim} N(0, \sigma_e^2)$. We place similar priors on α , β , and σ_e^2 regardless of the other model components. Thus, $\alpha \sim N(0, \sigma_a^2)$, $\beta \sim N(0, \sigma_b^2 I_{p \times p})$, and $\sigma_e^2 \sim IG(a_e, b_e)$ where σ_a^2 and σ_b^2 are fixed and set to something large, $I_{p \times p}$ denotes a $p \times p$ identity matrix, and IG denotes the inverse gamma distribution. We take a_e and b_e to be fixed as well and set them to something small, 0.01 for example.

For M total smoothed effects and F total functional effects, a general additive model might have the form

$$y_i = \alpha + \beta' \mathbf{x}_i + \sum_{m=1}^M s_m(z_{im}) + \sum_{f=1}^F \int_{t \in \mathcal{T}} w_{if}(t) \gamma_f(t) dt + \epsilon_i, \quad (1)$$

where $s_m(z_{im})$ is a smoothed effect and $\gamma_f(t)$ is a functional effect. The functional effects, as written, are over the same time domain although this does not have to be the case, i.e. t and \mathcal{T} can vary with f . The covariates z_{im} and $w_{if}(t)$ are not part of \mathbf{x}_i which is a vector of scalar covariates. The vector β contains the scalar effects and α is the model intercept.

Using basis expansions to represent each smoothed and functional effect, the matrix version of Equation (1) is

$$\mathbf{Y} = \alpha \mathbf{1} + X\beta + \sum_{m=1}^M \Xi_m \zeta_m + \sum_{f=1}^F W_f \Theta_f \lambda_f + \epsilon, \quad (2)$$

where \mathbf{Y} and ϵ are both $n \times 1$ vectors and X is an $n \times (P - 1)$ matrix of scalar effects. Considering the smoothed model components first: for K knots, Ξ_m is the $n \times K$ matrix containing the basis-expanded representation of the z_{im} , $i = 1, \dots, n$, and ζ_m is the $K \times 1$ vector of basis coefficients. For the functional components, let Θ_f be a $T \times L$ matrix of basis functions and let λ be a $L \times 1$ vector of basis coefficients. Then W_f is the $n \times T$ matrix containing the functional covariate. Both smoothed and functional effects use a B-spline basis expansion. Under empirical testing, we found that $K = 8$ knots works well for smoothed effects and $L = 12$ works best for

functional effects. In Equation (2), we use the basis expansion $\gamma = \Theta\lambda$ where γ is the $T \times 1$ vector of functional coefficients, $\gamma(t)$. Goldsmith et al. [2011] implement a similar approach for variational scalar-on-function regression.

All basis expanded effects, both smoothed and functional, require penalization to avoid overfitting. It is well known that penalized regression models can be represented as mixed models [Ruppert et al., 2003, Chapter 4]. In the Frequentist context, this means the components one wishes to penalize are treated as random effects. However, there is no distinction between random and fixed effects in the Bayesian context as any unknown parameter is treated as if it is random and has a prior placed on it. Thus, the equivalent is a prior specification that introduces the penalty. Because of the relationship between mixed effects models and penalized smoothing, we can leverage existing algorithms for mean field variational mixed effect models to estimate Equation (2). Ormerod and Wand [2010] provide one such algorithm which forms the basis of our estimation procedure for the variational additive model.

We place a mean-zero shrinkage prior on the elements of ζ_m of the form $\zeta_m \sim N(\mathbf{0}, \omega_m \mathcal{P}_m)$ where ω_m is a tuning parameter and $\mathbf{0}$ is a $K \times 1$ vector of zeros. The matrix \mathcal{P}_m is a $K \times K$ penalty matrix which is the difference operator in matrix form, see Eilers and Marx [1996] for more details. The prior on the basis expanded functional effects is similar: $\lambda_f \sim N(\mathbf{0}, \eta_f \Delta_f)$ where η_f is a tuning parameter and $\mathbf{0}$ is an $L \times 1$ vector of zeros. We distinguish the penalty matrix for the functional effect, Δ_f , because it has a different form than in the smoothed case: $\Delta_f = \xi \Delta_0 + (1 - \xi) \Delta_2$ where Δ_0 is the zeroth derivative matrix and Δ_2 is the second derivative matrix of the B-spline basis function. This penalty matrix is consistent with other penalized functional regression settings including Goldsmith and Kitago [2016] and Meyer et al. [2022].

Regardless of effect type, the tuning parameters need to be estimated to induce shrinkage. Thus, we place conditionally conjugate inverse-gamma priors on all ω_m and η_f : $\omega_m \sim IG(a_{\omega,m}, b_{\omega,m})$ and $\eta_m \sim IG(a_{\eta,m}, b_{\eta,m})$. We set the hyper-parameters $a_{\omega,m}$, $b_{\omega,m}$, $a_{\eta,m}$, and $b_{\eta,m}$, to something small, 0.01 or less. Since these parameters are tuning parameters, it is reasonable to place a weakly informative prior on each. However, our formulation does allow for differing amounts of information to be passed to different components when the model contains multiple smoothed and functional effects. The Directed Acyclic Graph (DAG) describing the Markov Blanket for this model is in Figure 1.

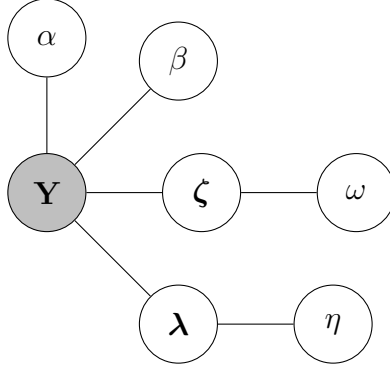


Figure 1: DAG for Gaussian variational additive model

Combining the above model specifications, the resulting q densities for MFVB approximation are

$$\begin{aligned}
 q(\boldsymbol{\theta}) &\sim N \left[\boldsymbol{\mu}_{q(\boldsymbol{\theta})}, \boldsymbol{\Sigma}_{q(\boldsymbol{\theta})} \right] \\
 q(\sigma_e^2) &\sim IG \left[a_e + \frac{N}{2}, B_{q(\sigma_e^2)} \right], \\
 q(\omega_1) &\sim IG \left[a_{\omega,1} + \frac{K}{2}, B_{q(\omega_1)} \right], \\
 &\dots \\
 q(\omega_M) &\sim IG \left[a_{\omega,M} + \frac{K}{2}, B_{q(\omega_M)} \right], \\
 q(\eta_1) &\sim IG \left[a_{\eta,1} + \frac{L}{2}, B_{q(\eta_1)} \right], \\
 &\dots \\
 q(\eta_F) &\sim IG \left[a_{\eta,F} + \frac{L}{2}, B_{q(\eta_F)} \right],
 \end{aligned}$$

depending on the number of smoothed (M) and functional (F) components in the model. The subscript- $q(\cdot)$ notation indicates the parameter to which the quantity belongs under the mean field approximation. The vector $\boldsymbol{\theta}$ contains all mean model parameters, i.e. $\boldsymbol{\theta} = [\alpha \ \beta \ \boldsymbol{\zeta}_1 \ \dots \ \boldsymbol{\zeta}_M \ \boldsymbol{\lambda}_1 \ \dots \ \boldsymbol{\lambda}_F]'$. Let \mathbf{C} denote the design matrix for Equation (2), that is $\mathbf{C} = [\mathbf{1} \ X \ \Xi_1 \ \dots \ \Xi_M \ W_1 \ \dots \ W_F]$. Algorithm 1 describes the estimation procedure. Convergence is determined

when changes in $\log[\underline{p}(\mathbf{Y}; q)]$ become negligible, where

$$\begin{aligned}
\log[\underline{p}(\mathbf{Y}; q)] &= \frac{1}{2}(P + K + L) - \frac{N}{2} \log(2\pi) \\
&\quad - \frac{P}{2} \log(\sigma_b^2) + \frac{1}{2} \log \left(|\Sigma_{q(\boldsymbol{\theta})}| \right) \\
&\quad - \frac{1}{2\sigma_b^2} \left[\boldsymbol{\mu}_{q(\alpha, \boldsymbol{\beta})}' \boldsymbol{\mu}_{q(\alpha, \boldsymbol{\beta})} + \text{tr} \left\{ \Sigma_{q(\alpha, \boldsymbol{\beta})} \right\} \right] \\
&\quad - a_e \log(b_e) - \left(a_e + \frac{N}{2} \right) \log(B_{q(\sigma^2)}) \\
&\quad + \log \left\{ \Gamma \left(a_e + \frac{N}{2} \right) \right\} - \log \{ \Gamma(a_e) \} \\
&\quad + \sum_{m=1}^M \left[a_{\omega, m} \log(b_{\omega, m}) \right. \\
&\quad \quad - \left(a_{\omega, m} + \frac{K}{2} \right) \log(B_{q(\omega_m)}) \\
&\quad \quad + \log \left\{ \Gamma \left(a_{\omega, m} + \frac{K}{2} \right) \right\} \\
&\quad \quad \left. - \log \{ \Gamma(a_{\omega, m}) \} \right] \\
&\quad + \sum_{f=1}^F \left[a_{\eta, f} \log(b_{\eta, f}) \right. \\
&\quad \quad - \left(a_{\eta, f} + \frac{L}{2} \right) \log(B_{q(\eta_f)}) \\
&\quad \quad + \log \left\{ \Gamma \left(a_{\eta, f} + \frac{L}{2} \right) \right\} \\
&\quad \quad \left. - \log \{ \Gamma(a_{\eta, f}) \} \right].
\end{aligned}$$

The algorithm is written generally and can be used to estimate parameters from Equation (1) for an arbitrary number of smoothed and functional effects.

Algorithm 1 Estimate Equation (1) components. The abbreviations ‘bd’ is for block diagonal.

Require: $B_{q(\omega_1)}, \dots, B_{q(\omega_M)}, B_{q(\eta_1)}, \dots, B_{q(\eta_F)} > 0$, and $\epsilon > 0$, small

1: **while** $\Delta \log[p(\mathbf{Y}; q)] > \epsilon$ **do**

2: $\mathcal{D} \leftarrow \text{bd} \left\{ (\sigma_b^2)^{-1} I_{p \times p}, \frac{a_{\omega,1} + \frac{K}{2}}{B_{q(\omega_1)}} \mathcal{P}_1, \dots, \frac{a_{\omega,M} + \frac{K}{2}}{B_{q(\omega_M)}} \mathcal{P}_M, \frac{a_{\eta,1} + \frac{L}{2}}{B_{q(\eta_1)}} \Delta_1, \dots, \frac{a_{\eta,F} + \frac{L}{2}}{B_{q(\eta_F)}} \Delta_M \right\}$

3: $\Sigma_{q(\boldsymbol{\theta})} \leftarrow \left[\frac{a_e + \frac{N}{2}}{B_{q(\sigma_e^2)}} \mathbf{C}' \mathbf{C} + \mathcal{D} \right]^{-1}$

4: $\boldsymbol{\mu}_{q(\boldsymbol{\theta})} \leftarrow \left(\frac{a_e + \frac{N}{2}}{B_{q(\sigma_e^2)}} \right) \Sigma_{q(\boldsymbol{\theta})} \mathbf{C}' \mathbf{Y}$

5: $B_{q(\sigma^2)} \leftarrow b_e + \frac{1}{2} \left[\left\{ \mathbf{Y} - \mathbf{C} \boldsymbol{\mu}_{q(\boldsymbol{\theta})} \right\}' \left\{ \mathbf{Y} - \mathbf{C} \boldsymbol{\mu}_{q(\boldsymbol{\theta})} \right\} + \text{tr} \{ \mathbf{C}' \mathbf{C} \} \Sigma_{q(\boldsymbol{\theta})} \right]$

6: **if** $M \geq 1$ **then**

7: **loop** $m = 1, \dots, M$

8: $B_{q(\omega_m)} \leftarrow b_{\omega,m} + \frac{1}{2} \left[\boldsymbol{\mu}_{q(\boldsymbol{\zeta}_m)}' \boldsymbol{\mu}_{q(\boldsymbol{\zeta}_m)} + \text{tr} \left\{ \frac{a_{\omega,m} + \frac{K}{2}}{B_{q(\omega_m)}} \mathcal{P}_m \right\} \right]$

9: **end loop**

10: **end if**

11: **if** $F \geq 1$ **then**

12: **loop** $f = 1, \dots, F$

13: $B_{q(\eta_f)} \leftarrow b_{\eta,f} + \frac{1}{2} \left[\boldsymbol{\mu}_{q(\boldsymbol{\lambda}_f)}' \boldsymbol{\mu}_{q(\boldsymbol{\lambda}_f)} + \text{tr} \left\{ \frac{a_{\eta,f} + \frac{L}{2}}{B_{q(\eta_f)}} \Delta_f \right\} \right]$

14: **end loop**

15: **end if**

16: **end while**

2.2.2 Binary Outcome

Suppose instead that y_i is a binary outcome for subjects $i = 1, \dots, n$. As in the Gaussian case, \mathbf{x}_i is a vector of scalar covariates that is $p \times 1$, α is the intercept, and $\boldsymbol{\beta}$ is $p \times 1$ vector where both α and $\boldsymbol{\beta}$ are non-smoothed, non-functional effects. Prior specification for these components are the same as in Section 2.2.1. To model the binary outcome, we use the latent variable representation which has the form

$$y_i = \begin{cases} 0 & y_i^* < 0 \\ 1 & y_i^* \geq 0, \end{cases} \quad (3)$$

for the latent variable $y_i^* \in \mathbb{R}$. That is, the binary outcome y_i only represents the observable part of a continuous, underlying process. We use the model from Equation (1) in the latent space:

$$y_i^* = \alpha + \boldsymbol{\beta}' \mathbf{x}_i + \sum_{m=1}^M s_m(z_{im}) + \sum_{f=1}^F \int_{t \in \mathcal{T}} w_{if}(t) \gamma_f(t) dt + \epsilon_i^*. \quad (4)$$

Assuming that the latent errors, ϵ_i^* , are Gaussian induces the probit link, i.e. $\epsilon_i^* \stackrel{iid}{\sim} N(0, 1)$. Since the representation in Equation (3) is scale-invariant, the variance of the latent variable is taken to be 1, see Albert and Chib [1993] for additional details on the Bayesian probit model.

Because we model in the latent space, the formulation follows analogously to that in Section 2.2.1. Thus, the vectorized version of the latent model is

$$\mathbf{Y}^* = \alpha \mathbf{1} + X \boldsymbol{\beta} + \sum_{m=1}^M \Xi_m \boldsymbol{\zeta}_m + \sum_{f=1}^F W_f \Theta_f \boldsymbol{\lambda}_f + \boldsymbol{\epsilon}^*,$$

where \mathbf{Y}^* and $\boldsymbol{\epsilon}^*$ are both $n \times 1$ vectors and the remaining model components are as previously defined. We place the same mean-zero shrinkage priors and hyper-priors on the probit model as we do for the Gaussian model: $\boldsymbol{\zeta}_m \sim N(\mathbf{0}, \omega_m \mathcal{P}_m)$, $\boldsymbol{\lambda}_f \sim N(\mathbf{0}, \eta_f \Delta_f)$, $\omega_m \sim IG(a_{\omega, m}, b_{\omega, m})$, and $\eta_m \sim$

$IG(a_{\eta,m}, b_{\eta,m})$. We also set the hyper-parameters $a_{\omega,m}$, $b_{\omega,m}$, $a_{\eta,m}$, and $b_{\eta,m}$, to something small, 0.01 or less for this model as well.

The addition of the latent variable, y_i^* , to model makes this model tractable and the resulting full conditionals are fully identifiable. Thus, the CAVI algorithm is a reasonable approach to performing estimation in the variational context. The q densities that result from the MFVB approximation are

$$\begin{aligned}
q(\boldsymbol{\theta}) &\sim N \left[\boldsymbol{\mu}_{q(\boldsymbol{\theta})}, \boldsymbol{\Sigma}_{q(\boldsymbol{\theta})} \right] \\
q(\mathbf{Y}^* | \mathbf{Y} = 0) &\sim N_{(-\infty, 0)} \left[\boldsymbol{\mu}_{q(\mathbf{Y}^*)}, I_{n_0 \times n_0} \right] \\
q(\mathbf{Y}^* | \mathbf{Y} = 1) &\sim N_{[0, \infty)} \left[\boldsymbol{\mu}_{q(\mathbf{Y}^*)}, I_{n_1 \times n_1} \right] \\
q(\omega_1) &\sim IG \left[a_{\omega,1} + \frac{K}{2}, B_{q(\omega_1)} \right], \\
&\dots \\
q(\omega_M) &\sim IG \left[a_{\omega,M} + \frac{K}{2}, B_{q(\omega_M)} \right], \\
q(\eta_1) &\sim IG \left[a_{\eta,1} + \frac{L}{2}, B_{q(\eta_1)} \right], \\
&\dots \\
q(\eta_F) &\sim IG \left[a_{\eta,F} + \frac{L}{2}, B_{q(\eta_F)} \right],
\end{aligned}$$

where n_0 is the number of failures and n_1 is the number of successes observed in y_i . The distributions $q(\mathbf{Y}^* | \mathbf{Y} = 0)$ and $q(\mathbf{Y}^* | \mathbf{Y} = 1)$ are conditional on the components of \mathbf{Y} that equal zero and one, respectively, and the subscripts $(-\infty, 0)$ and $[0, \infty)$ denote truncation of the distribution to those ranges. Thus, $q(\mathbf{Y}^* | \mathbf{Y} = 0)$ and $q(\mathbf{Y}^* | \mathbf{Y} = 1)$ are truncated normal distributions. Because the Markov blanket for the penalized components of the binary model are the same as in the Gaussian model, the q densities for the penalty terms are the same in both, see Figure 2 which contains the DAG for the binary model.

Algorithm 2 describes the CAVI-based estimation approach. Convergence

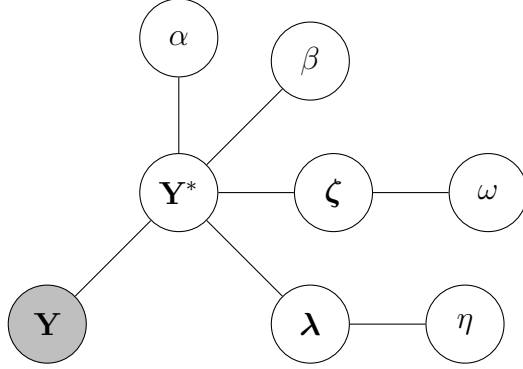


Figure 2: DAG for probit variational additive model

is determined when changes in $\log[p(\mathbf{Y}; q)]$ become negligible:

$$\begin{aligned}
\log[p(\mathbf{Y}; q)] &= \mathbf{Y}' \log[\Phi\{\mathbf{C}\boldsymbol{\mu}_q(\boldsymbol{\theta})\}] \\
&+ (\mathbf{1} - \mathbf{Y})' \log[\mathbf{1} - \Phi\{\mathbf{C}\boldsymbol{\mu}_q(\boldsymbol{\theta})\}] - \frac{1}{2} \log |\boldsymbol{\Sigma}_q(\boldsymbol{\theta})| \\
&- \frac{1}{2\sigma_b^2} \left[\boldsymbol{\mu}_{q(\alpha, \boldsymbol{\beta})}' \boldsymbol{\mu}_{q(\alpha, \boldsymbol{\beta})} + \text{tr} \left\{ \boldsymbol{\Sigma}_{q(\alpha, \boldsymbol{\beta})} \right\} \right] \\
&+ \sum_{m=1}^M \left[a_{\omega, m} \log(b_{\omega, m}) \right. \\
&\quad - \left(a_{\omega, m} + \frac{K}{2} \right) \log(B_{q(\omega_m)}) \\
&\quad + \log \left\{ \Gamma \left(a_{\omega, m} + \frac{K}{2} \right) \right\} \\
&\quad \left. - \log\{\Gamma(a_{\omega, m})\} \right] \\
&+ \sum_{f=1}^F \left[a_{\eta, f} \log(b_{\eta, f}) \right. \\
&\quad - \left(a_{\eta, f} + \frac{L}{2} \right) \log(B_{q(\eta_f)}) \\
&\quad + \log \left\{ \Gamma \left(a_{\eta, f} + \frac{L}{2} \right) \right\} \\
&\quad \left. - \log\{\Gamma(a_{\eta, f})\} \right],
\end{aligned}$$

where $\Phi(\cdot)$ denotes the cdf of a standard Gaussian distribution. The algorithm can accommodate an arbitrary number of smoothed and functional effects when fitting the binary model described by Equations (3) and (4).

Algorithm 2 Estimate components from Equations (3) and (4). The abbreviations ‘bd’ is for block diagonal. $\Phi(\cdot)$ denotes the cdf of a standard Gaussian distribution and $\phi(\cdot)$ denotes the pdf.

Require: $B_{q(\omega_1)}, \dots, B_{q(\omega_M)}, B_{q(\eta_1)}, \dots, B_{q(\eta_F)} > 0$, and $\epsilon > 0$, small. Set $\boldsymbol{\mu}_{q(\mathbf{Y}^*)}$ to something reasonable, e.g. $\mathbf{0}$.

```

1: while  $\Delta \log[p(\mathbf{Y}; q)] > \epsilon$  do
2:    $\mathcal{D} \leftarrow \text{bd} \left\{ (\sigma_b^2)^{-1} I_{p \times p}, \frac{a_{\omega,1} + \frac{K}{2}}{B_{q(\omega_1)}} \mathcal{P}_1, \dots, \frac{a_{\omega,M} + \frac{K}{2}}{B_{q(\omega_M)}} \mathcal{P}_M, \frac{a_{\eta,1} + \frac{L}{2}}{B_{q(\eta_1)}} \Delta_1, \dots, \frac{a_{\eta,F} + \frac{L}{2}}{B_{q(\eta_F)}} \Delta_M \right\}$ 
3:    $\boldsymbol{\Sigma}_q(\boldsymbol{\theta}) \leftarrow [\mathbf{C}'\mathbf{C} + \mathcal{D}]^{-1}$ 
4:    $\boldsymbol{\mu}_q(\boldsymbol{\theta}) \leftarrow \boldsymbol{\Sigma}_q(\boldsymbol{\theta})\mathbf{C}'\mathbf{Y}$ 
5:    $\boldsymbol{\mu}_{q(\mathbf{Y}^*)} \leftarrow \mathbf{C}'\boldsymbol{\mu}_q(\boldsymbol{\theta}) + \phi[\mathbf{C}'\boldsymbol{\mu}_q(\boldsymbol{\theta})] / \Phi[\mathbf{C}'\boldsymbol{\mu}_q(\boldsymbol{\theta})]^{\mathbf{Y}} [\Phi\{\mathbf{C}'\boldsymbol{\mu}_q(\boldsymbol{\theta})\} - \mathbf{1}]^{(1-\mathbf{Y})}$ 
6:   if  $M \geq 1$  then
7:     loop  $m = 1, \dots, M$ 
8:        $B_{q(\omega_m)} \leftarrow b_{\omega,m} + \frac{1}{2} \left[ \boldsymbol{\mu}_q(\boldsymbol{\zeta}_m)' \boldsymbol{\mu}_q(\boldsymbol{\zeta}_m) + \text{tr} \left\{ \frac{a_{\omega,m} + \frac{K}{2}}{B_{q(\omega_m)}} \mathcal{P}_m \right\} \right]$ 
9:     end loop
10:  end if
11:  if  $F \geq 1$  then
12:    loop  $f = 1, \dots, F$ 
13:       $B_{q(\eta_f)} \leftarrow b_{\eta,f} + \frac{1}{2} \left[ \boldsymbol{\mu}_q(\boldsymbol{\lambda}_f)' \boldsymbol{\mu}_q(\boldsymbol{\lambda}_f) + \text{tr} \left\{ \frac{a_{\eta,f} + \frac{L}{2}}{B_{q(\eta_f)}} \Delta_f \right\} \right]$ 
14:    end loop
15:  end if
16: end while

```

3 Variational ZLS Tests

Zhang et al. [2000] and Zhang and Lin [2003] discuss hypothesis testing for comparing two or more semiparametric curves. The test statistic, which we refer to as the ZLS test, requires the existence of a vector, $\mathbf{c}(z)$, such that the estimate of a semiparametric function, $s(z)$, can be written as $\hat{s}(z) = \mathbf{c}(z)' \mathbf{Y}$ at some value $z \in [\min_i(z_i), \max_i(z_i)]$. We develop the testing

framework first for the estimated variational smoothed functions and then for variational scalar-on-function regression curves. Without loss of generality, each test is formulated for a generic effect and we will perform the tests one at a time.

3.1 Smoothed Effects

Under the null and regardless of outcome type, we assume the smoothed component has no effect, i.e. $H_0 : s(z) = 0 \forall z$. The alternative is then that there is a non-zero effect for some values of z . To test this null, we derive a ZLS-like test which requires a vector $\mathbf{c}(z)$:

Proposition 1. *Upon convergence of Algorithm 1, there exists a vector $\mathbf{c}(z)$ such that $\hat{s}(z) = \mathbf{c}(z)'Y$.*

Proof. Let $\Sigma_{q(\zeta)}$ denote the converged covariance matrix for the smoothed effect ζ resulting from Algorithm 1. That is, $\Sigma_{q(\zeta)}$ is the principal submatrix of $\Sigma_{q(\theta)}$ that corresponds to ζ . Upon convergence, the quantity $\mathbf{c}(z) = \left(\frac{a_e + \frac{N}{2}}{B_{q(\sigma_e^2)}}\right) \Sigma_{q(\zeta)} \Xi$ is a vector such that $\hat{s}(z) = \mathbf{c}(z)'Y$. \square

Zhang and Lin [2003] describe the implementation of the ZLS test for non-Gaussian outcomes that formulates the vector $\mathbf{c}(z)$ in terms of the working model. In the binary case, the working model is represented by the latent variable \mathbf{Y}^* .

Proposition 2. *Upon convergence of Algorithm 2, there exists a vector $\mathbf{c}(z)$ such that $\hat{s}(z) = \mathbf{c}(z)'\mathbf{Y}^*$.*

Proof. Let $\Sigma_{q(\zeta)}$ denote the converged covariance matrix for the smoothed effect ζ resulting from Algorithm 2. Thus, $\Sigma_{q(\zeta)}$ is the principal submatrix of $\Sigma_{q(\theta)}$ that corresponds to ζ . Upon convergence, the quantity $\mathbf{c}(z) = \Sigma_{q(\zeta)} \Xi$ is a vector such that $\hat{s}(z) = \mathbf{c}(z)'\mathbf{Y}^*$. \square

The statistic for the ZLS test of a variational smoothed effect is then

$$G_s(\mathbf{Y}) = \int_{z(1)}^{z(N)} \mathbf{Y}'\mathbf{c}(z)\mathbf{c}(z)'\mathbf{Y}dz = \mathbf{Y}'U\mathbf{Y}, \quad (5)$$

where $U = \int_{z_{(1)}}^{z_{(N)}} \mathbf{c}(z)\mathbf{c}(z)'dz$, $z_{(1)} = \min_i(z_i)$, and $z_{(N)} = \max_i(z_i)$. When $\mathbf{c}(z)$ arises from the binary model in Algorithm 2, we replace \mathbf{Y} with \mathbf{Y}^* in Equation (5). Consistent with Zhang et al. [2000] and Zhang and Lin [2003], we approximate the distribution of $G(\mathbf{Y})$ and $G_s(\mathbf{Y}^*)$ as a scaled chi-squared, using the Satterthwaite approximation [Satterthwaite, 1943].

Under H_0 , the mean and variance of both $G_s(\mathbf{Y})$ and $G_s(\mathbf{Y}^*)$ are $e_s = \mathbf{E}'U\mathbf{E} + tr(UV)$ and $\psi_s = 2tr\{(UV)^2\} + 4\mathbf{E}'UVU\mathbf{E}$ where \mathbf{E} is the mean vector of \mathbf{Y} (or \mathbf{Y}^*) and V is the covariance matrix—in the binary case, V is a working covariance matrix. Under the null, $U\mathbf{E}$ is negligible, so we approximate these quantities with $e_s \approx tr(UV)$ and $\psi_s \approx 2tr\{(UV)^2\}$. Setting the approximate versions of e_s and ψ_s equal to the mean and variance of a scaled chi-squared, $\kappa_s\chi_{\nu_s}^2$, results in a scaling factor of $\kappa_s = \psi_s/(2e_s)$ and a degrees of freedom of $\nu_s = 2e_s^2/\psi_s$. The p -value for the test can be approximated by finding $Pr[\chi_{\nu_s}^2 > G_s(\mathbf{Y})/\kappa_s]$.

3.2 Functional Effects

We now extend the ZLS test to a functional effect. The null for this component is $H_0 : \gamma(t) = 0 \forall t \in \mathcal{T} = \{t : t = t_1, \dots, t_T\}$. We assume that the functional effect is measured on a grid that can be equally spaced, although it is not required to be. The test requires $\mathbf{c}(t)$ such that $\hat{\gamma}(t) = \mathbf{c}(t)'\mathbf{Y}$ for some time point $t \in \mathcal{T}$.

Proposition 3. *Upon convergence of Algorithm 1, there exists a vector $\mathbf{c}(t)$ such that $\hat{\gamma}(t) = \mathbf{c}(t)'\mathbf{Y}$.*

Proof. Let $\Sigma_{q(\gamma)}$ denote the converged covariance matrix for the smoothed functional effect γ resulting from Algorithm 1. That is, $\Sigma_{q(\gamma)}$ is the principal submatrix of $\Sigma_{q(\theta)}$ that corresponds to γ . Upon convergence, the quantity

$$\mathbf{c}(t) = \left(\frac{a_e + \frac{N}{2}}{B_{q(\sigma_e^2)}} \right) \Sigma_{q(\gamma)} W \Theta \text{ is a vector such that } \hat{\gamma}(t) = \mathbf{c}(t)'\mathbf{Y}. \quad \square$$

Similar to the Gaussian case, the test in the binary setting requires a vector $\mathbf{c}(t)$ such that $\hat{\gamma}(t) = \mathbf{c}(t)'\mathbf{Y}^*$ where \mathbf{Y}^* is from the working model.

Proposition 4. *Upon convergence of Algorithm 2, there exists a vector $\mathbf{c}(t)$ such that $\hat{\gamma}(t) = \mathbf{c}(t)'\mathbf{Y}^*$.*

Proof. Let $\Sigma_q(\gamma)$ denote the converged covariance matrix for the smoothed functional effect γ resulting from Algorithm 2. Thus, $\Sigma_q(\gamma)$ is the principal submatrix of $\Sigma_q(\theta)$ that corresponds to γ . Upon convergence, the quantity $\mathbf{c}(t) = \Sigma_q(\gamma)W\Theta$ is a vector such that $\hat{\gamma}(t) = \mathbf{c}(t)'\mathbf{Y}^*$. \square

The statistic for the functional effect requires only slight alteration from Equation 5:

$$G(\mathbf{Y}) = \int_{t_1}^{t_T} \mathbf{Y}'\mathbf{c}(t)\mathbf{c}(t)'\mathbf{Y}dt = \mathbf{Y}'Q\mathbf{Y},$$

where $Q = \int_{t_1}^{t_T} \mathbf{c}(t)\mathbf{c}(t)'\mathbf{Y}dt$. A similar approximation to that used for the smoothed effect results in the p -value having the form $Pr \left[\chi_{\nu_\gamma}^2 > G_\gamma(\mathbf{Y})/\kappa_\gamma \right]$ where $\kappa_\gamma = \psi_\gamma/(2e_\gamma)$ and a degrees of freedom of $\nu_\gamma = 2e_\gamma^2/\psi_\gamma$. Once again, when the outcome is binary, we replace \mathbf{Y} with \mathbf{Y}^* in the formulation of the statistic. Under H_0 , the approximations to the mean and variance are $e_\gamma \approx tr(QV)$ and $\psi_\gamma \approx 2tr \{(QV)^2\}$ where V is the covariance of \mathbf{Y} or working covariance of \mathbf{Y}^* , depending on the outcome type.

4 Empirical Study

To evaluate the tests proposed in Section 3, we consider testing a single smoothed effect or functional effect at a time. For smoothed effects, we generate models of the form

$$y_i = \alpha + s(z_i) + \epsilon_i \text{ and } y_i^* = \alpha + s(z_i) + \epsilon_i.$$

In the functional case, we generate models using

$$y_i = \alpha + \int_{t \in \mathcal{T}} w_i(t)\gamma(t)dt + \epsilon_i \text{ and}$$

$$y_i^* = \alpha + \int_{t \in \mathcal{T}} w_i(t)\gamma(t)dt + \epsilon_i.$$

Under both, $\epsilon_i \stackrel{iid}{\sim} N(0, 1)$ and y_i^* is the latent variable from the binary model in Equation (3). We examine type I error and power for sample sizes of $N = 50, 100$, and 200.

Under both outcome types, the functional form of $s()$ is based on either the negated cdf of a standard normal to give a decreasing sigmoidal effect, Φ , or the pdf of a gamma distribution with both parameters set to 2, Γ , which produces a non-central, skewed peak. Thus,

$$s(z_i) = -\Phi\left(\frac{z_i - 0.5}{0.5}\right) \text{ or } s(z_i) = \frac{2^2}{\Gamma(2)} z_i e^{-2z_i}.$$

Both “true” effect types were chosen to mimic the observed smoothed effects in the lidar and ragweed data, respectively, which we analyze in Section 5. When generating data using a true Φ curve, we take z_i from a $N(0, 1)$ and when generating under the Γ curve, we take x_i from a χ_1^2 .

The functional effects are either a two peak effect constructed by adding two Gaussian pdfs together or a seasonal effect based on a sin curve. The curves are then either

$$\begin{aligned} \gamma(t) &= \frac{1}{4} \sqrt{\frac{100}{2\pi}} \exp\left\{-\frac{100}{2} \left(t - \frac{1}{4}\right)^2\right\} \\ &\quad + \frac{1}{8} \sqrt{\frac{100}{2\pi}} \exp\left\{-\frac{100}{2} \left(t - \frac{3}{4}\right)^2\right\} \text{ or} \\ \gamma(t) &= \sin\{\pi(4t - 1)\} \left(t + \frac{1222}{10000}\right). \end{aligned}$$

The grid is taken to be on the unit interval, $\mathcal{T} = (0, 1)$, with equally spaced points of size $T = 50$ or 100 . To generate $w_i(t)$, we use a Gaussian process centered at $\gamma(t)$ with an auto-regressive 1 covariance structure and correlation set to $\rho = 0.5$.

4.1 Type I Error

Type I error rates for the various settings and outcome types can be found in Tables 1 and 2 and are based on 1000 simulated datasets. In general, the choice of knots varies by effect type (smoothed or functional) and outcome type (Gaussian or binary). For smoothed effects on Gaussian outcomes, preliminary testing found that $K = 8$ knots worked well across all settings and produced the well controlled type I error rates from Table 1. Under the binary outcome, we found that $K = 6$ knots was preferable for controlling type I error across most settings. Error rates tend to increase as N increases

Table 1: Type I error for smoothed effect using the nominal α of 0.05. Abbreviations: Out. is for Outcome, Gauss. is for Gaussian, and Bin. is for Binary.

Out.	Curve	Sample Size		
		50	100	200
Gauss.	Φ	0.019	0.035	0.050
	Γ	0.027	0.031	0.045
Bin.	Φ	0.004	0.022	0.058
	Γ	0.007	0.020	0.031

and for the binary case can be quite small for the smallest N . Decreasing K when N is small does give rates closer to nominal, which we study in Section 4.3.

For the functional effects in Table 2, we observe a similar pattern to the smoothed case. Type I error rates are smallest when N is small and move toward nominal as N increases. Once again, when the outcome is binary, we see the test is quite conservative for the two smaller sample sizes of $N = 50$ and 100. Knot choice in the functional case also depends on outcome type with $L = 12$ knots performing well in preliminary testing for Gaussian outcomes and $L = 9$ performing well for binary outcomes across all settings. Lowering L can improve type I error when the sample size is smaller. We explore this further in Section 4.3.

4.2 Power

To evaluate power, we scale the curves $s(z_i)$ and $\gamma(t)$ by a factor, $\xi = 1, 3$, or 5. For the smoothed effects, consistent with the type I error evaluation, we use $K = 8$ and 6 knots for Gaussian and binary models, respectively. For the functional effects, we use $L = 12$ and 9 for Gaussian and binary models, respectively. Tables 3 and 4 contain power for all settings except for the binary model with a functional effect for $N = 50$ since this setting requires fewer knots.

The tests for smoothed effects gains power as N increases, regardless of outcome type (Table 3). For the same number of knots used to examine type I error, power is lower when N is small but increases as ξ gets larger. The

Table 2: Type I error for functional effects using the nominal α of 0.05. Abbreviations: Out. is for Outcome, Gauss. is for Gaussian, and Bin. is for Binary.

Out.	Curve	T	Sample Size		
			50	100	200
Gauss.	Two Peak	50	0.029	0.042	0.052
		100	0.049	0.054	0.051
	Seas.	50	0.029	0.042	0.052
		100	0.049	0.054	0.051
Bin.	Two Peak	50	0.009	0.016	0.048
		100	0.005	0.012	0.055
	Seas.	50	0.009	0.016	0.048
		100	0.005	0.012	0.055

Table 3: Power for smoothed effects using the nominal α of 0.05. Abbreviations: Out. is for Outcome, Gauss. is for Gaussian, and Bin. is for Binary.

Out.	Curve	N	ξ		
			1	3	5
Gauss.	Φ	50	0.092	0.962	1.000
		100	0.456	1.000	1.000
		200	0.624	1.000	1.000
	Γ	50	0.060	0.692	0.998
		100	0.170	0.986	1.000
		200	0.336	1.000	1.000
Bin.	Φ	50	0.018	0.152	0.256
		100	0.103	0.516	0.672
		200	0.309	0.862	0.938
	Γ	50	0.032	0.262	0.386
		100	0.120	0.568	0.716
		200	0.278	0.848	0.954

Table 4: Power for functional effects using the nominal α of 0.05 when $T = 50$. Abbreviations: Out. is for Outcome, Gauss. is for Gaussian, and Bin. is for Binary.

Out.	Curve	N	ξ		
			1	3	5
Gauss.	Two Peak	50	1.000	1.000	1.000
		100	1.000	1.000	1.000
		200	1.000	1.000	1.000
	Seas.	50	0.998	1.000	1.000
		100	1.000	1.000	1.000
		200	1.000	1.000	1.000
Bin.	Two Peak	100	0.160	0.996	1.000
		200	0.874	1.000	1.000
	Seas.	100	0.100	0.912	0.996
		200	0.608	1.000	1.000

tests tend to perform better in the Gaussian case when testing smoothed effects, although for large N the binary model achieves reasonable levels of power. Power is similar between the two curve types.

For functional effects, we see that power increases quickly as ξ increases, regardless of outcome type (Table 4). As with the smoothed case, power improves as N increases as well. The curve type does not have much of an impact on power for larger values of ξ . The Gaussian case in particular achieves a high level of power quite quickly. Missing from Table 4 is the power under the $N = 50$ case for the binary outcome. The number of knots that generally gave good type I error, $L = 9$, is too large for the smaller sample case when evaluating power. Thus, we defer an exploration of this setting to Section 4.3. Table 4 displays power when $T = 50$. We also evaluated the $T = 100$ case and found good power for Gaussian outcomes under all N and the binary outcomes when $N = 100$ and 200. Results from that simulation are in Section 1 of the Supplementary Material.

Table 5: Power for binary models using the nominal $\alpha = 0.05$ when $N = 50$. Functional effects were generated under the $T = 50$ setting. Abbreviations: Smo. is for smoothed, Func. is for functional, and Kn. is for knots— K for smoothed effects, L for functional effects.

Effect	Curve	Kn.	ξ			
			0	1	3	5
Smo.	Φ	4	0.037	0.210	0.686	0.832
		5	0.004	0.022	0.152	0.256
	Γ	4	0.018	0.152	0.582	0.774
		5	0.007	0.032	0.262	0.386
Func.	DN	6	0.034	0.344	0.994	1.000
		7	0.017	0.166	0.914	0.920
	Seas.	6	0.034	0.144	0.854	0.982
		7	0.017	0.048	0.278	0.406

4.3 Small Sample Binary Model

When the outcome is binary and $N = 50$, Tables 1 and 2 suggest a very conservative test. Our power evaluation reflects this conservatism in the smoothed case. For functional effects, we omit the results under $L = 9$ knots due to model instability. As we now demonstrate, the binary case is sensitive to not only the sample size but the number of knots. When $N = 50$, lowering L for functional effects or K for smoothed effects will improve the type I error rate and power.

Table 5 contains type I error and power for both smoothed and functional effects when the outcome is binary and the sample size is smaller. We consider $K = 4$ and 5 knots in the smoothed case and $L = 6$ and 7 knots in the functional cases. Type I error is the table value when $\xi = 0$, otherwise the power evaluation is the same as in Tables 3 and 4. All testing is performed at the $\alpha = 0.05$ level.

When the sample size is small, the test obtains closer to nominal type I error with smaller numbers of knots: $K = 4$ for smoothed effects and $K = 6$ knots for functional effects. The test is still conservative, but less so when compared to the results from Tables 1 and 2. The power gain is noticeable, particularly for the functional effects where $L = 6$ knots achieves

Table 6: ZLS test results for the data illustrations. All tests are performed at the $\alpha = 0.05$ level. Abbreviations: Rag. denotes ragweed, Stront. denotes strontium, DiS denotes day-in-season.

Data	N	Variable	$\chi^2 (\nu)$	p -value
Lidar	221	$s(\text{range}_i)$	6.77 (1.32)	0.015
Rag.	335	$s_1(\text{DiS}_i)$	35.7 (1.73)	< 0.001
		$s_2(\text{temp}_i)$	1.49 (1.19)	0.271
Stront.	106	$s(\text{age}_i)$	3.19 (1.29)	0.106
Flight	26	$\Delta\text{SaO}_2_i(t)$	0.56 (1.41)	0.601
DTI	99	$\text{CCA}_i(t)$	9.02 (2.56)	0.020

power when $N = 50$ similar to what we observe for larger values of N . This is under the $T = 50$ case. As T increases, however, more knots are needed. When $T = 100$, for example, $L = 7$ knots produces a closer to nominal type I error while $L = 6$ knots can result in inflated type I error—see Section 1 of the Supplementary Material for additional details.

The number of knots we use in Sections 4.1 and 4.2 work in general for most problems. But as can be seen from Table 5 as well as the additional results in the Supplementary Material, care must be taken when selecting the number of knots for binary outcome models with smaller sample sizes.

5 Data Illustrations

We demonstrate the use of the variational ZLS test in five data settings that cover a wide spectrum of substantive fields. We consider three smoothed estimation problems and two scalar-on-function regression problems. Two of the five datasets have binary outcomes while the rest have Gaussian outcomes. Test results are in Table 6 and some graphical results are provided below. Additional graphical results are in the Supplementary Material, including graphs of the changes in the ELBO for each model. Code to implement our models is available for download as an R package from <https://github.com/markjmeyer/fitVAM>.

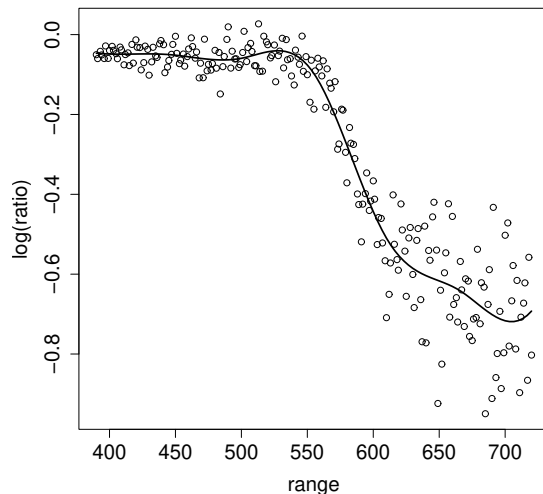


Figure 3: Estimated semiparametric curve, $\hat{s}(\text{range}_i)$, for the lidar data model.

5.1 Smoothing Problems

5.1.1 Lidar Data

The lidar data is a classic illustration of semiparametric regression used by Ruppert et al. [2003] to illustrate the concept. It features 221 observations from a light detection and ranging experiment measuring the log of the ratio of light received from two laser sources. The predictor of interest in this example is the distance travelled before the light is reflected back to its source. The data comes from a text on spectroscopic techniques [Sigrist, 1994] and is available in the R package `SemiPar` [Wand, 2018]. We fit the model

$$\log(\text{ratio}_i) = \alpha + s(\text{range}_i) + \epsilon_i,$$

where $\epsilon_i \sim N(0, \sigma^2)$, using Algorithm 1 and use the variational ZLS test from Section 3 to perform a test of the null hypothesis $H_0 : s(\text{range}_i) = 0$ for all values of range_i .

The results of the test are in Table 6. The estimated curve is in Figure 3. Given the smoothed effect and Gaussian outcome, we use $K = 8$ knots in

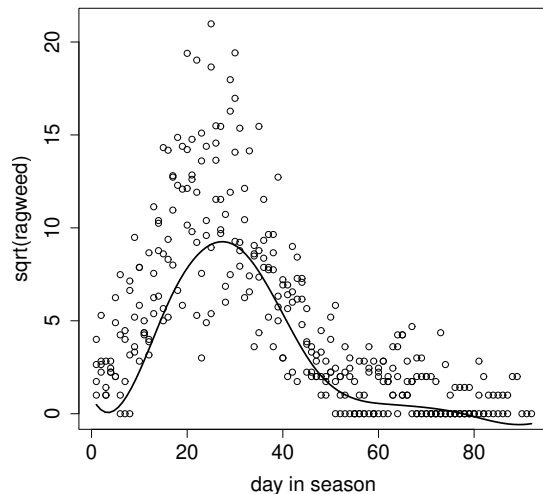


Figure 4: Estimated semiparametric curve, $\hat{s}_1(\text{DiS}_i)$, for the ragweed data model.

modeling. The resulting curve captures the nature of the relationship in the data quite well, Figure 3. Based on the ZLS test results in Table 6, there appears to be a significant association between range and log-ratio ($\chi^2_{1.32} = 6.77$, $p = 0.015$).

5.1.2 Ragweed Data

Stark et al. [1997] describe determinants of ragweed levels for 335 days in the city of Kalamazoo, Michigan, USA. Included in the data are the day in the current ragweed pollen season the measurement was taken on and temperature, among others. The former variable gives a sense of how far along in the pollen, i.e. allergy, season the measurement was taken. The data is available in the R package `SemiPar` [Wand, 2018]. We jointly estimate smoothed effects for both variables predicting the square root of ragweed levels:

$$\sqrt{\text{ragweed}_i} = \alpha + s_1(\text{DiS}_i) + s_2(\text{temp.}_i) + \epsilon_i,$$

where $\epsilon_i \sim N(0, \sigma^2)$, DiS denotes day in season, and temp. denotes temperature. Estimation is performed using Algorithm 1 on $K = 8$ knots and we

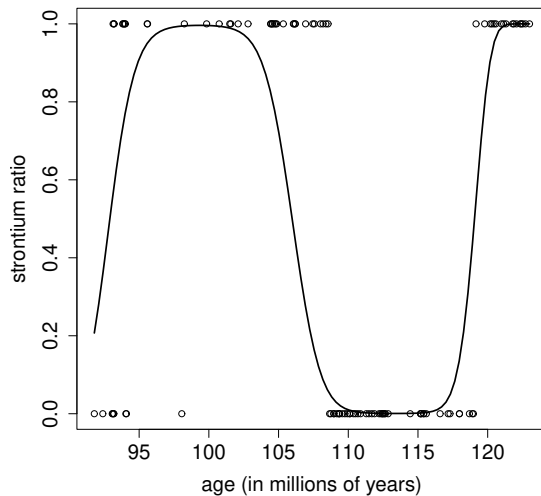


Figure 5: Estimated semiparametric curve, $\hat{s}_1(\text{age}_i)$, for the ragweed data model.

test both the null of $H_0 : s(\text{DiS}_i) = 0$ and $H_0 : s(\text{temp}_i) = 0$.

Table 6 displays the results of the variational ZLS test while Figure 4 contains the estimated curve for day in season, i.e. $\hat{s}_1(\text{DiS}_i)$. The graph of the estimated effect of temperature is in the Supplementary Material. Even in the presence of temperature, day in season is a highly significant predictor of the ragweed level at the nominal α level ($\chi_{1.73}^2 = 35.7, p < 0.001$). Temperature, on the other hand, is not a significant predictor. If we fit the model with temperature alone, we find moderate significance at the $\alpha = 0.05$ level ($\chi_{1.11}^2 = 4.69, p = 0.036$).

5.1.3 Strontium Data

We now examine a binary outcome model from a study of fossils looking at the ratios of strontium isotopes from mid-cretaceous deep-sea sections [Bralower et al., 1997]. The study examined the ratio of two strontium isotopes in relation to the age (in millions of years) of the sample. We discretize the outcome to below median strontium ratio (coded as 0) versus above median strontium ratio (coded as 1) and analyze the effect of age using the

latent model

$$y_i^* = \alpha + s(\text{age}_i) + \epsilon_i^*,$$

where $\epsilon_i^* \sim N(0, 1)$.

We obtain estimates via Algorithm 2 on $K = 6$ knots and perform the ZLS to test the null that $H_0 : s(\text{age}_i) = 0$ at the nominal level. The results of the test are in Table 6 while the estimated curve is in Figure 5. While we do not find evidence of a statistically significant relationship between the ratios of strontium isotopes and the age of the sample ($\chi_{1,29}^2 = 3.19$, $p = 0.106$), the estimated curve fits the discretized data quite well.

5.2 Functional Problems

5.2.1 Flight Health Data

Meyer et al. [2019] describes a study of the impact of exposure to altitude in commercial flight on in-flight markers of heart health finding that exposure to altitude negatively impacts some markers, including heart rate. Using this data, we examine the impact of exposure to altitude for 310 minutes on post-flight heart rate. Exposure to altitudes in commercial flights is known to decrease blood oxygen saturation SaO_2 . We use five-minute SaO_2 measurements to examine post-flight heart rate. The study was a cross-over design with patients having one day at altitude and one day at sea level in a hypobaric pressure chamber (the order of treatment arms was block randomized). To account for the pairing, we pre-difference both the SaO_2 curves and post-experimental condition heart rate. The model is then

$$\Delta hr_i = \alpha + \int_{t \in \mathcal{T}} \Delta \text{SaO}_2(t) \gamma(t) dt + \epsilon_i,$$

where $\epsilon_i \sim N(0, \sigma^2)$, and Δ denotes the change in the variable. For estimation via Algorithm 1, we employ 12 knots. We performed the differencing by taking active treatment (at altitude) minus placebo (at sea level). From table 6, we lack evidence to suggest there is an association between changes in blood oxygen level in flight on changes in heart rate post-flight, from altitude to sea level ($\chi_{1,41}^2 = 0.56$, $p = 0.601$).

5.2.2 DTI Data

Our last illustration looks at the impact of a diffusion tensor image fractional anisotropy tract profiles from the corpus callosum on paced auditory serial addition test (PASAT) scores in patients with multiple sclerosis. This data has been considered as a functional data example by Goldsmith et al. [2011] and Goldsmith et al. [2012], among others. We first discretize the PASAT score to below median (coded as 0) and above median (coded as 1). Lower PASAT scores are associated with cognitive impairment. This binary variable serves as our outcome with the latent model

$$y_i^* = \alpha + \int_{t \in \mathcal{T}} \text{CCA}_i(t) \gamma(t) dt + \epsilon_i^*,$$

where $\epsilon_i^* \sim N(0, 1)$ and CCA denotes the diffusion tensor image fractional anisotropy tract profiles from the corpus callosum. Although the ZLS test on variational binary functional models can be conservative for $N = 100$ (see Table 2), we use $L = 9$ knots for this analysis. Table 6 displays the results which suggests an association between the tract profiles and whether or not the PASAT score was high or low ($\chi_{2.56}^2 = 9.02$, $p = 0.020$).

6 Discussion

As variational techniques gain popularity, additional methods will be required to ensure that statistical inference can be confidently performed within the framework. We show that for MFVB approximations to Gaussian and binary additive models, the CAVI algorithms admit forms that can be used to implement a global test of a smoothed effect, upon convergence of the algorithm. We further demonstrate that the penalized spline representation of the functional effect in these additive models also admits a form via the CAVI algorithm whereby one can construct a global test of a functional effect.

Our empirical evaluation demonstrates that the testing framework has good Frequentist properties in terms of type I error rate and power. The data illustrations show the test is applicable to a wide range of substantive questions with sample sizes varying from 26 to 335. While the choice of knots can impact type I error and power, particularly for the binary case, we identify a set of reasonable choices for the number knots depending on the outcome, effect type, sample size, and grid (in the functional case).

Our work is applied to MFVB approximations for Gaussian and binary additive models using the product density transformation. Other transformations may admit similar forms, for example the tangent transformation. The work of Luts and Wand [2015], which examines semiparametric models for Poisson and negative binomially distributed outcomes, may also be amenable. Recent work to improve variance estimation by Giordano et al. [2018] could also present useable forms for ZLS-like tests. These other transformations and approaches are of interest for future work to demonstrate the applicability of the test within the broader variational framework.

Supplementary information

Further results from our empirical study and data illustrations are in the Supplementary Material accompanying this manuscript.

References

- J. Albert and S. Chib. Bayesian analysis of binary and polychotomous response data. *Journal of the American Statistical Association*, 88:669–679, 1993. doi: 10.1080/01621459.1993.10476321.
- P. Bickel, D. Choi, X. Chang, and H. Zhang. Asymptotic normality of maximum likelihood and its variational approximation for stochastic blockmodels. *The Annals of Statistics*, 41:1922–1943, 2013. doi: 10.1214/13-AOS1124.
- D. M. Blei, A. Kucukelbir, and J. D. McAuliffe. Variational inference: a review for statisticians. *Journal of the American Statistical Association*, 112:859–877, 2017.
- T. Bralower, P. Fullagar, C. K. Paull, G. S. Dwyer, and R. M. Leckie. Mid-Cretaceous strontium-isotope stratigraphy of deep-sea sections. *Geological Society of America Bulletin*, 109:1421–1442, 1997.
- Y. H. Chen, B. Mukherjee, S. D. Adar, V. J. Berrocal, and B. A. Coull. Robust distributed lag models using data adaptive shrinkage. *Biostatistics*, 19:461–478, 2018.

- C. Crainiceanu, C. Ruppert, G. Claeskens, and M. P. Wand. Exact likelihood ratio tests for penalised splines. *Biometrika*, 92:91–103, 2005. doi: 10.1093/biomet/92.1.91.
- C. M. Crainiceanu and D. Ruppert. Likelihood ratio tests in linear mixed models with one variance component. *Journal of the Royal Statistical Society: Series B*, 66:165–185, 2004. doi: 10.1111/j.1467-9868.2004.00438.x.
- P. H. C. Eilers and B. D. Marx. Flexible smoothing with b-splines and penalties. *Statistical Science*, 11:89–121, 1996. doi: 10.1214/ss/1038425655.
- A. Gelman, J. B. Carlin, H. S. Stern, D. B. Dunson, A. Vehtari, and D. B. Rubin. *Bayesian Data Analysis*. Chapman and Hall-CRC, Boca Raton, FL, 3rd edition, 2013.
- R. Giordano, T. Broderick, and M. I. Jordan. Covariances, robustness, and variational bayes. *Journal of Machine Learning Research*, 19:1–49, 2018.
- J. Goldsmith and T. Kitago. Assessing systematic effects of stroke on motor control using hierarchical function-on-scalar regression. *Journal of the Royal Statistical Society, Series C*, 65:215–236, 2016. doi: 10.1111/rssc.12115.
- J. Goldsmith, J. Bobb, C. M. Crainiceanu, B. Caffo, and D. Reich. Penalized functional regression. *Journal of Computational and Graphical Statistics*, 20:830–851, 2011. doi: 10.1198/jcgs.2010.10007.
- J. Goldsmith, C. Crainiceanu, B. Caffo, and D. Reich. Longitudinal penalized functional regression for cognitive outcomes on neuronal tract measurements. *Journal of the Royal Statistical Society, Series C*, 61:453–469, 2012. doi: 10.1111/j.1467-9876.2011.01031.x.
- J. Goldsmith, S. Greven, and C. Crainiceanu. Corrected confidence bands for functional data using principal components. *Biometrics*, 69:41–51, 2013. doi: 10.1111/j.1541-0420.2012.01808.x.
- S. Greven, C. M. Crainiceanu, H. Küchenhoff, and A. Peters. Restricted likelihood ratio testing for zero variance components in linear mixed models. *Journal of Computational and Graphical Statistics*, 17:870–891, 2008. doi: 10.1198/106186008X386599.

- F. K. C. Hui, C. You, H. L. Shang, and S. Müller. Semiparametric regression using variational approximations. *Journal of the American Statistical Association*, 114:1765–1777, 2019. doi: 10.1080/01621459.2018.1518235.
- A. E. Ivanescu, A.-M. Staicu, F. Scheipl, and S. Greven. Penalized function-on-function regression. *Computational Statistics*, 30:539–568, 2015. doi: 10.1007/s00180-014-0548-4.
- C. Y. Y. Lee and M. P. Wand. Variational methods for fitting complex bayesian mixed effects models to health data. *Statistics in Medicine*, 35:165–188, 2016. doi: 10.1002/sim.6737.
- H. Li, S. Kozey-Keadle, V. Kipnis, and R. J. Carroll. Longitudinal functional additive model with continuous proportional outcomes for physical activity data. *Stat*, 5:242–250, 2016. doi: 10.1002/sta4.121.
- J. Luts and M. P. Wand. Variational inference for count response semiparametric regression. *Bayesian Analysis*, 10:991–1023, 2015.
- W. Ma, L. Xiao, and B. Liu. A functional mixed model for scalar on function regression with application to a functional MRI study. *Biostatistics*, 22:439–454, 2021. doi: 10.1093/biostatistics/kxz046.
- E. J. Malloy, J. S. Morris, S. D. Adar, H. Suh, D. R. Gould, and B. A. Coull. Wavelet-based functional linear mixed models: an application to measurement error-corrected distributed lag models. *Biostatistics*, 11:432–452, 2010. doi: 10.1093/biostatistics/kxq003.
- M. W. McLean, G. Hooker, A.-M. Staicu, F. Scheipl, and D. Ruppert. Functional generalized additive models. *Journal of Computational and Graphical Statistics*, 23:249–269, 2014. doi: 10.1080/10618600.2012.729985.
- M. J. Meyer, B. A. Coull, F. Versace, P. Cinciripini, and J. S. Morris. Bayesian function-on-function regression for multi-level functional data. *Biometrics*, 71:563–574, 2015. doi: 10.1111/biom.12299.
- M. J. Meyer, I. Mordukhovich, G. A. Wellenius, M. A. Mittleman, J. P. McCracken, B. A. Coull, and E. McNeely. Changes in heart rate and rhythm during a crossover study of simulated commercial flight in older and vulnerable participants. *Frontiers Physiology*, 10:1339, 2019. doi: 10.3389/fphys.2019.01339.

- M. J. Meyer, J. S. Morris, R. P. Gazes, and B. A. Coull. Ordinal probit functional outcome regression with application to computer-use behavior in rhesus monkeys. *Annals of Applied Statistics*, 16:537–550, 2022. doi: 10.1214/21-AOAS1513.
- J. T. Ormerod and M. P. Wand. Explaining variational approximations. *The American Statistician*, 64:140–153, 2010.
- J. O. Ramsay and C. J. Dalzell. Some tools for functional data analysis. *Journal of the Royal Statistical Society, Series B*, 53:539–561, 1991. doi: 10.1111/j.2517-6161.1991.tb01844.x.
- J. O. Ramsay and B. W. Silverman. *Functional Data Analysis*. Springer, New York, 2nd edition, 2005.
- D. Ruppert, M. P. Wand, and R. J. Carroll. *Semiparametric regression*. Cambridge University Press, Cambridge, United Kingdom, 2003.
- F. E. Satterthwaite. An approximate distribution of variance components. *Biometrika*, 2:110–114, 1943.
- F. Scheipl, A.-M. Staicu, and S. Greven. Functional additive mixed models. *Journal of Computational and Graphical Statistics*, 24:477–501, 2015. doi: 10.1080/10618600.2014.901914.
- F. Scheipl, J. Gertheiss, and S. Greven. Generalized functional additive mixed models. *Electronic Journal of Statistics*, 10:1455–1492, 2016. doi: 10.1214/16-EJS1145.
- M. Sigrist, editor. *Air Monitoring by Spectroscopic Techniques (Chemical Analysis Series)*, volume 197. Wiley, New York, 1994.
- P. C. Stark, L. M. Ryan, J. L. McDonald, and H. A. Burge. Using meteorologic data to model and predict daily ragweed pollen levels. *Aerobiologia*, 13:177–184, 1997.
- M. Wand. *SemiPar: Semiparametric Regression*, 2018. URL <https://CRAN.R-project.org/package=SemiPar>. R package version 1.0-4.2.

- M. P. Wand. Fast approximate inference for arbitrarily large semiparametric regression models via message passing. *Journal of the American Statistical Association*, 112:137–168, 2017. doi: 10.1080/01621459.2016.1197833.
- Y. Wang and D. M. Blei. Frequentist consistency of variational bayes. *Journal of the American Statistical Association*, 114:1147–1161, 2019.
- T. Westling and T. H. McCormick. Beyond prediction: A framework for inference with variational approximations in mixture models. *Journal of Computational and Graphical Statistics*, 28:778–789, 2019. doi: 10.1080/10618600.2019.1609977.
- S. N. Wood. *Generalized Additive Models: An Introduction with R*. Chapman and Hall/CRCs, New York, 2nd edition, 2017. doi: 10.1201/9781315370279.
- F. Yang and Y. Yang. A sparse estimate based on variational approximations for semiparametric generalized additive models. *Computational Statistics*, 2024. doi: 10.1007/s00180-024-01485-2.
- Y. Yang, D. Pati, and A. Bhattacharya. α -variational inference with statistical guarantees. *The Annals of Statistics*, 48:886–905, 2020. doi: 10.1214/19-AOS1827.
- C. You, J. T. Ormerod, and S. Müller. On variational bayes estimation and variational information criteria for linear regression models. *Australian & New Zealand Journal of Statistics*, 56:73–87, 2014.
- A. Y. Zhang and H. H. Zhou. Theoretical and computational guarantees of mean field variational inference for community detection. *Annals of Statistics*, 48:2575–2598, 2020.
- D. Zhang and X. Lin. Hypothesis testing in semiparametric additive mixed models. *Biostatistics*, 4:57–74, 2003.
- D. Zhang, X. Lin, and M. Sowers. Semiparametric regression for periodic longitudinal hormone data from multiple menstrual cycles. *Biometrics*, 56:31–39, 2000.